Molecular Pharmacology Fast Forward. Published on February 13, 2015 as DOI: 10.1124/mol.114.096982
This article has not been copyedited and formatted. The final version may differ from this version.

Staurosporine induces formation of two types of extra-long cell protrusions: actin-based filaments and microtubule-based shafts

Takayuki Kohno, Takafumi Ninomiya, Shin Kikuchi, Takumi Konno, and Takashi Kojima

Department of Cell Science, Research Institute for Frontier Medicine (T. K., T. K., T. K.), and Department of Anatomy (T. N., S. K.), Sapporo Medical University, Japan

Molecular Pharmacology Fast Forward. Published on February 13, 2015 as DOI: 10.1124/mol.114.096982
This article has not been copyedited and formatted. The final version may differ from this version.

Running title: Staurosporine extends two types of extra-long protrusions

Corresponding author: Takayuki Kohno, Department of Cell Science, Research Institute for Frontier Medicine, Sapporo Medical University, Minami-1, Nishi-17, Chuo-ku, Sapporo 060-8556, Japan. Tel: +81-11-611-2111, Fax: +81-11-611-2299, e-mail: kohno@sapmed.ac.jp

Number of text pages: 39

Number of tables: 0

Number of figures: 7 (besides 3 supplemental tables, 2 supplemental figures, and 4 supplemental videos)

Number of references: 49

Number of words in Abstract: 214

Number of words in Introduction: 536

Number of words in Discussion: 1426

Abbreviations: AF, actin filament; CA, constitutive active; CD, cytochalasin D; 2-DG, 2-deoxyglucose; DN, dominant negative; DPI, diphenylene iodide; IF, intermediate filament; Jsp, jasplakinolide; LatA, latrunculin A; MF, microfilament; MT, microtubule; Myo10, myosin-X; Noc, nocodazole; STS, staurosporine; TEM, transmission electron microscopy; TNT, tunneling nanotube.

Molecular Pharmacology Fast Forward. Published on February 13, 2015 as DOI: 10.1124/mol.114.096982
This article has not been copyedited and formatted. The final version may differ from this version.

Abstract

Staurosporine (STS) has been known as a classical PKC inhibitor and is a broad-spectrum inhibitor targeting over 250 protein kinases. In this study, we observed that STS treatment induced drastic morphological changes such as elongation of a very large number of non-branched, actin-based long cell protrusions that reached up to 30 μm in an hour without caspase activation or PARP cleavage in fibroblasts and epithelial cells. These cell protrusions were elongated not only from the free cell edge but also from the cell-cell junctions. The elongation of STS-dependent protrusions was required for ATP hydrolysis and was dependent on Myo10 and fascin, but independent of Cdc42 and VASP. Interestingly, in the presence of an actin polymerization inhibitor, namely cytochalasin D, latrunculin A, or jasplakinolide, STS treatment induced excess tubulin polymerization, which resulted in the formation of many extra-long microtubule (MT)-based protrusions towards the outside of the cell. The unique MT-based protrusions were thick and linear compared to the STS-induced filaments or stationary filopodia. These protrusions composed of microtubules have been scarcely observed in cultured non-neuronal cells. Taken together, our findings revealed that STS-sensitive kinases are essential for maintenance of normal cell morphology, and a common unidentified molecular mechanism is involved in the formation of following two different types of protrusions: actin-based filaments and MT-based shafts.

Molecular Pharmacology Fast Forward. Published on February 13, 2015 as DOI: 10.1124/mol.114.096982
This article has not been copyedited and formatted. The final version may differ from this version.

Introduction

Spatiotemporal regulation of cell protrusion is involved in the morphological dynamics. Cellular protrusions are formed mainly through elongation of cytoskeletal filaments in the extracellular direction, and universally observed during differentiation, proliferation, migration, apoptosis, and expression of physiological function in living cells. Several types of cell protrusions have been observed including filopodia, microvilli, stereocilia, bristle, invadopodia, podosome, tunneling nanotube (TNT), microtentacle (McTN), and nerve axon (Murphy and Courtneidge, 2011), (Revenu *et al.*, 2004), (Charpentier *et al.*, 2014). Representative components of cytoskeleton include actin, tubulin, and vimentin, which form distinct types of cytoskeletal filament, actin filament (AF), microtubule (MT), and intermediate filament (IF), respectively (Blanchoin *et al.*, 2014). Coordinate rearrangement of cytoskeletal filaments are required for the active morphological changes of growing cells.

The length of AFs depends on the balance between stabilization and destabilization of actin polymerization, which are regulated by adaptor proteins such as actin-modulating proteins (Rotty *et al.*, 2013). To date, actin-modulating proteins reported include profilin and thymosin β4 as G-actin binding proteins, cofilin/ADF as a depolymerizing protein, CAPZ as a capping protein, Arp2/3 complex as a branching protein, fascin as a bundling protein, and VASP and formin as polymerization promoting proteins (dos Remedios *et al.*, 2003). These adaptor proteins are modulated by Rho family small GTPases including Rho, Rac, and Cdc42, as well as kinases and phosphatases regulated by these GTPases, and contribute to the spatiotemporal

Molecular Pharmacology Fast Forward. Published on February 13, 2015 as DOI: 10.1124/mol.114.096982
This article has not been copyedited and formatted. The final version may differ from this version.

dynamics of the cytoskeleton (Heasman and Ridley, 2008). The AF length control mechanism mostly remains to be elucidated (Mogilner and Rubinstein, 2005). Interestingly, the presence of long filopodia reaching a length up to 150 μm has also been demonstrated in the development process of the limb bud (Sanders *et al.*, 2013). These long filopodia are considered to be small GTPase-independent protrusions (Gousset *et al.*, 2013).

MT dynamics are also regulated through the stabilization/destabilization balance. MTs assume two forms depending on location of the initiation point, centrosomal MT and non-centrosomal MT, and the both forms require stabilization of the MT minus end for formation of the initiation point. γ-Tubulin ring complex (γTuRC) contributes to stabilization of the minus end in the centrosomal MT form (Kollman *et al.*, 2011), while CAMSAP3 has been identified as a stabilization factor for the non-centrosomal MT form (Meng *et al.*, 2008). In MTs with the stabilized minus end, their length is controlled by dynamic instability between polymerization and depolymerization of the plus end (van der Vaart *et al.*, 2009).

Since actin and tubulin tend to polymerize non-enzymatically and spontaneously, cells are equipped with complicated molecular systems for efficient regulation of polymerization and depolymerization. Many of these regulatory factors are modulated by protein phosphorylation (Govek *et al.*, 2005). Therefore, universal inhibition of these kinases appears to allow for observation of cell morphology in the absence of physiological regulation. To prove this hypothesis, we observed morphological changes of cells using staurosporine (STS), which has been known as a

Molecular Pharmacology Fast Forward. Published on February 13, 2015 as DOI: 10.1124/mol.114.096982
This article has not been copyedited and formatted. The final version may differ from this version.

classical PKC inhibitor and is a broad-spectrum inhibitor targeting over 250 protein kinases (Karaman *et al.*, 2008). The STS-treated cells showed elongation of a very large number of non-branched, actin-based protrusions reaching a length as long as 30 μm in an hour. These protrusions extended from the contact area between cells, and no retraction was observed. Interestingly, we found that combination of STS and an actin polymerization inhibitor promoted tubulin polymerization, resulting in formation of cellular protrusions with a new morphology of extremely long-, MT-based protrusions. These protrusions composed of microtubules have seldom been observed in cultured non-neuronal cells. We propose that there is a previously unidentified mechanism to regulate the length and composition of protrusions involved in the STS-sensitive factors.

Molecular Pharmacology Fast Forward. Published on February 13, 2015 as DOI: 10.1124/mol.114.096982
This article has not been copyedited and formatted. The final version may differ from this version.

Materials and methods

Reagents and plasmids

All reagents and plasmids used in this study are listed in Electronic Supplementary Material Tables S1, S2 and S3. All primers were obtained from Sigma-Aldrich (St. Louis, MO). All PCR products were completely sequenced.

Cell culture and transfections

HeLa, 3Y1, COS7, HepG2 and H1299 cells were cultured in DMEM supplemented with 10% fetal bovine serum, 100 U/ml penicillin and 100 μg/ml streptomycin at 37°C, 5% CO_2. Primary human nasal epithelial cells were prepared as previously described (Someya *et al.*, 2013). Lipofectamine plus reagent (Invitrogen, Carlsbad, CA) and RNAiMAX reagent (Invitrogen) were used for plasmid and siRNA transfection, respectively, according to the manufacturer's instructions. For RNA interference experiments, HeLa cells were plated at 1 x 10^5 cells per well of a 24-well plate. The cells were used 48-72 hours after siRNA transfection. For STS treatment, cells grown on a glass bottom dish (Iwaki) or a glass cover slip (Matsunami, Japan) were gently washed once with glucose free Krebs solution (KH buffer; 120 mM NaCl, 5 mM KCl, 0.62 mM $MgSO_4$, 1.8 mM $CaCl_2$, 10 mM HEPES, pH 7.2) at room temperature, then treated with the indicated concentrations of STS in the absence or presence of the indicated compounds at room temperature for the indicated times. The cells were then used for the experiments as described below.

Molecular Pharmacology Fast Forward. Published on February 13, 2015 as DOI: 10.1124/mol.114.096982
This article has not been copyedited and formatted. The final version may differ from this version.

Live-cell imaging and Immunofluorescence microscopy

For live-cell imaging, the cells prepared as described above were placed under atmospheric conditions at room temperature on the microscope stage. Images were acquired with the LSM-510 META microscope system (Carl Zeiss, Thornwood, NJ) employing the channel mode or the lambda mode using a Plan-Apochromat 63x/1.40 Oil DIC M27 oil immersion objective, and zen software (Carr Zeiss). For fixed-cell imaging, the cells prepared as described above were fixed in an equal volume of 10% trichloroacetic acid (Sigma-Aldrich) for 20 min at room temperature, then washed four times with PBS, followed by permeabilization for 2 min in PBS containing 0.5% saponin (ICN, Costa Mesa, CA) and 1% fatty acid free BSA (Sigma-Aldrich). Primary and secondary antibodies were diluted in Can Get Signal solution (Toyobo, Japan). The cell staining was performed at room temperature in the dark for 60 min. H33342 was added to the secondary antibody staining solution. The coverslips were mounted in Mowiol 4-88 (Calbiochem, San Diego, CA) with DABCO (Sigma). Fixed samples were imaged as described above. Live-cell images, fixed-cell images, and time-lapse movies were processed using ImageJ program with self-written macros. Figures were generated with Adobe Photoshop CS6 and Illustrator CS6. The length and number of cell protrusions were measured using ImageJ, and represented as a dot-plot (modified scatter plot) in Microsoft Excel using self-written macros. The Student's t-test was done based on 30 randomly chosen data sets from all raw data using Stat Plus software (AnalystSoft) with self-written macros.

Molecular Pharmacology Fast Forward. Published on February 13, 2015 as DOI: 10.1124/mol.114.096982
This article has not been copyedited and formatted. The final version may differ from this version.

Transmission electron microscopy (TEM)

TEM samples were prepared as described previously (Someya *et al.*, 2013). In brief, cells grown on 8-well chamber slides were treated with STS, then fixed in an equal volume of 5% glutaraldehyde/0.1 M PBS (pH 7.3) overnight at 4°C, postfixed in 2% osmium tetroxide in the same buffer, dehydrated in a graded ethanol series and embedded in Epon 812. Ultrathin sections were then cut on a Sorvall Ultramicrotome MT-5000 (Dupont-Sorvall, Newtown, CT). The sections were stained with uranyl acetate followed by lead citrate and examined at 80 kV with a transmission electron microscope (H7500; Hitachi, Japan).

Immunoblotting

Cells were washed twice with cold PBS, and lysed in extraction buffer (50 mM Tric-HCl, pH7.5, 150 mM NaCl, 2 mM Vanadate, 1 mM EDTA, Complete protease inhibitor cocktail (Roche), 0.1% NP40), followed by centrifugation at 20,000 x g for 15 min at 4°C. The resulting supernatant was analyzed by SDS-PAGE, and transferred to a PVDF membrane, then washed in TBS-T (10 mM Tris-HCl, pH7.5, 100 mM NaCl, 0.1% Tween20) and blocked with 1% nonfat milk in TBS-T for 5 min at 65°C. The blotted membrane was incubated with a primary antibody for 1 h at RT or overnight at 4°C, followed by incubation with a peroxidase-conjugated secondary antibody for 1 h at RT. Signals were detected with ECL-plus reagent (GE Healthcare, Piscataway, NJ) in LAS1000 (Fuji, Japan).

Molecular Pharmacology Fast Forward. Published on February 13, 2015 as DOI: 10.1124/mol.114.096982
This article has not been copyedited and formatted. The final version may differ from this version.

Results

STS induces elongation of many long cell protrusions

We observed STS-induced morphological changes in multiple cells in their living state, and found common features thereof. For example, a 30-minute treatment of HeLa cells with STS at room temperature induced marked elongation of many non-branched, long cell protrusions (Fig. 1A). Such long cell protrusions were not formed under experimental conditions that did not contain STS (Fig. 1B). Time-lapse images of STS-treated cells indicated that the STS-induced protrusions extended while continuously moving to and fro without any retraction (Fig. 1C, Movie 1 and 2). In the absence of the cell membrane dye FM1-43, the elongation rate of these protrusions was 0.82 μm/min 30 minutes after STS addition and decreased over time (Fig. 1D), but spontaneous vibration was observed even more than 4 hours after the addition of STS. The length of the elongated protrusions was dependent on the STS concentration ranging from 25 nM to 1 μM (Fig. 1E). Many of known cell protrusions are formed in membrane regions not in contact with other cells (Vasioukhin *et al.*, 2000). Interestingly, the STS-induced protrusions were also formed from regions involved in cell-to-cell contact (Fig. 1F). These STS-dependent changes in cell morphology have also been observed in rat fibroblast cell 3Y1 (Fig. 1G), African Green Monkey SV40-transfected kidney fibroblast cell COS7 (Fig. 1H), human liver cancer cell HepG2 (Fig. 1I), human non-small-cell lung cancer cell H1299 (Fig. 1J), and primary human nasal epithelial cells (Fig.S1). From these results, STS was demonstrated to induce morphological

Molecular Pharmacology Fast Forward. Published on February 13, 2015 as DOI: 10.1124/mol.114.096982
This article has not been copyedited and formatted. The final version may differ from this version.

changes of marked elongation of many long cell protrusions in a short period of time in multiple cell types.

Cell protrusions that elongate in an STS-dependent manner are composed of actin filaments

Despite the fact that STS shows the inhibitory activity against many kinases including PKC, no long protrusion was observed in the presence of another protein kinase inhibitor as indicated in Fig. 2 (each left panels), and moreover co-treatment with STS and the indicated inhibitor did not repress the elongation of STS-dependent protrusions (each right graph). STS has also been known to induce Caspase-3/7-dependent apoptosis (Jiang *et al.*, 2013), but no increase in Caspase-3/7 activity was observed within the time range 0 to 4 hours required for the elongation of STS-dependent protrusion (Fig. 3A). To clarify the constituents of the STS-dependent cell protrusion, we observed the cells using transmission electron microscopy (TEM). As shown in Fig. 3B, these protrusions formed on HeLa cells were suggested to contain many long actin filaments (left panel, arrows). These filaments were oriented parallel to the direction of the elongation and little branch was observed. No long protrusion was observed in control (right panel). To identify that the protrusions are composed of actin filaments, the cells were transfected with GFP-actin plasmid, and its intracellular localization in living cells was observed with a confocal microscope. In steady-state HeLa cells, GFP-actin was shown to localize at focal contacts and stress fibers or distribute diffusely in the cytoplasm (Fig. 3C, lower panels). On the other hand, in the

Molecular Pharmacology Fast Forward. Published on February 13, 2015 as DOI: 10.1124/mol.114.096982
This article has not been copyedited and formatted. The final version may differ from this version.

presence of STS, GFP-actin was not only strongly localized in the vicinity of cell margins, but also distributed over the entire region of long protrusions (Fig. 3C, upper panels). In addition, the actin stress fibers observed before addition of STS disappeared upon addition of STS. STS did not induce an appreciable change in the shape of the nucleus within the observation period. Next, we observed endogenous actin localization. Since STS-induced protrusions were susceptible to aldehyde fixation and alcohol fixation (unpublished observations), the cells were fixed with TCA in this experiment (Hayashi *et al.*, 1999). While antibodies to endogenous actin recognize both F-actin and G-actin in TCA-fixed cells, actin was strongly localized to the cell margins under the conditions of this experiment (Fig. 3D, right panel). In the presence of STS, endogenous actin, like GFP-actin described above, was distributed in the vicinity of cell margins and over the entire elongating region of protrusions (Fig. 3D, left panel). From these results, cell protrusions that extremely elongate in an STS-dependent manner were demonstrated to be filopodia-like protrusions composed of actin filaments.

ATP supply is required for the elongation of STS-dependent cell protrusions

Supply of actin monomers bound by ATP is essential for polymerization of actin (Pollard, 1986). ATP is produced through both oxidative phosphorylation and glucose metabolism, and the increased ATP level is linked with accelerated cell functions (Vander Heiden *et al.*, 2009). Since STS inhibits kinase activity nonselectively and broadly, STS treatment was predicted to cause an increase in the intracellular ATP level. Before investigating whether STS changes the intracellular ATP level, we

Molecular Pharmacology Fast Forward. Published on February 13, 2015 as DOI: 10.1124/mol.114.096982
This article has not been copyedited and formatted. The final version may differ from this version.

examined whether the cellular ATP content was maintained by either oxidative phosphorylation or aerobic glycosylation. As shown in Fig. 4A, the intracellular ATP level decreased to 15% of the initial level in the presence of the glucose metabolism inhibitor 2-deoxyglucose (2-DG) for 2 hours as indicated in magenta, while control was maintained at 90% or higher (in green). Therefore, ATP production in these cells was found to be almost entirely dependent on glucose metabolism. Then, we observed morphological changes occurring in ATP-depleted cells upon STS administration. As shown in Fig. 4B, STS-dependent, markedly long protrusions were not formed in the presence of 2-DG compared to the absence of 2-DG (Fig. 4D). 2-DG caused little morphological change in steady-state cells (Figs. 4, C and E). Next, we investigated whether STS induced an increase in the intracellular ATP level. As shown in Fig. 4F, STS treatment resulted in an immediate consumption of approximately 10% of ATP followed by a modest decline, but at least STS treatment did not increase the total intracellular ATP level under the above-mentioned conditions (open and closed triangles). We had tried to search for additional intracellular ATP-depleting agents in our preliminary trial and successfully found that the NADPH oxidase inhibitor diphenylene iodide (DPI) depleted intracellular ATP in HeLa cells. As shown in Fig. 4F, the ATP level reduced through the administration of DPI (open circles) was restored by the addition of glucose (closed circles). Therefore, we used DPI for a recoverable ATP-depleting reagent. We then observed morphological changes occurring in these cells upon administration of STS. DPI caused almost no morphological changes in steady-state HeLa cells (Fig. 4G). STS administration in the presence of DPI resulted in

Molecular Pharmacology Fast Forward. Published on February 13, 2015 as DOI: 10.1124/mol.114.096982
This article has not been copyedited and formatted. The final version may differ from this version.

complete inhibition of the elongation of STS-dependent protrusions, and the cells showed healthy cell morphology similar to that of the control (Fig. 4H). This inhibitory effect was eliminated by the addition of glucose (Fig. 4I). With respect to characteristics of the protrusions observed here, no significant difference was found in the length or number of protrusions (Fig. 4J, lane 6) compared to the absence of DPI (Fig. 4J, lane 2). In addition, the loading of glucose without DPI did not affect the length or number of STS-induced protrusions (Fig. 4J, lane 3). From these results, ATP was found essential for the elongation of STS-dependent protrusions. Our data also revealed that the broad inhibition of kinases by STS does not necessarily immediately trigger accumulation of intracellular ATP.

Myo10 and fascin are involved in the elongation of STS-dependent cell protrusions

Many actin-modulating proteins related to the formation of filopodia have been reported to date (dos Remedios *et al.*, 2003). To investigate whether these proteins are involved in the elongation of STS-dependent protrusions, we knocked down some actin-modulating proteins using siRNA in HeLa cells (Fig. 5A). As shown in Fig. 5B, elongation of protrusions was significantly inhibited in Myo10- (lane 3) and fascin- (lane 4) knockdown cells compared with the control (lane 2), while the elongation was not inhibited by the knockdown of Cdc42 (lane 5), VASP (lane 6), profilin (lane 7) and cofilin (lane 8). An additive effect was observed for inhibition of the extension of protrusions by double knockdown of Myo10 and fascin (lane 9). This effect was not significant but obviously showed a trend ($p > 0.05$). Interestingly, the inhibition was

Molecular Pharmacology Fast Forward. Published on February 13, 2015 as DOI: 10.1124/mol.114.096982
This article has not been copyedited and formatted. The final version may differ from this version.

eliminated by double knockdown of Myo10 and Cdc42 (lane 10). No additive effect was observed for double knockdown of VASP (lane 11), profilin (lane 12), and cofilin (lane 13), and Myo10. Fascin and Myo10 have been reported to localize to the entire protrusion and the tip of the filopodia, respectively (Nagy *et al.*, 2008). These results indicate that STS induces the elongation of long protrusions by promoting actin polymerization involving Myo10 and accelerating convergence of actin filaments involving fascin, but the elongation was independent of Cdc42, VASP, cofilin and profilin.

An actin polymerization inhibitor induces elongation of thick cell protrusions in the co-presence of STS

With the expectation that the actin polymerization inhibitor Cytochalasin D (CD) prevents the formation of STS-dependent protrusions, we administered STS and CD simultaneously to steady-state HeLa cells and observed the cell morphology in the living state 2 hours after administration in the presence of FM1-43 using a confocal microscope. The result showed that the cell protrusions did not disappear upon co-administration of STS and CD (Fig. 6A). No appreciable change in cell morphology was observed with CD alone (Fig. 6B). Under these experimental conditions, no significant change in the shape of the nucleus was observed. It was noteworthy that the protrusions induced with the combination of two compounds (Fig. 6C) were thicker and straighter than the protrusions induced by STS alone (Fig. 6D) and the steady-state cell protrusions (Fig. 6E). The apparent diameters of these protrusions were measured in

Molecular Pharmacology Fast Forward. Published on February 13, 2015 as DOI: 10.1124/mol.114.096982
This article has not been copyedited and formatted. The final version may differ from this version.

confocal microscopy images (Fig. 6F). The diameter of the protrusions induced with the combination of STS and CD was significantly greater than the diameter of the protrusions induced by STS alone or in the steady-state (t-test, $p < 0.001$). The length of the protrusions induced by the combination of the two compounds was markedly longer ($p < 0.001$) than the steady-state cell protrusions, but significantly shorter ($p < 0.05$) than the protrusions induced by STS alone (Fig. 6G). Next we observed the elongation process of these protrusions continuously in living cells. Because cell membrane dyes FM1-43 and FM4-64 negatively affected the efficient elongation of protrusions (unpublished observations), we observed the process in HeLa cells expressing a GFP-fusion protein of PLC-delta1 PH domain (PH-GFP), which interacts specifically with cell membrane lipids (Yeung *et al.*, 2006). As shown in Fig. 6H and Movie 3, the protrusions elongated continuously without retraction in the co-presence of STS and CD in PH-GFP expressing cells, but were reduced in flexibility and the number of protrusions compared to the STS-induced ones (Fig. 1A), and terminated in a bulbous tip. These morphological changes were also observed in the presence of alternative actin polymerization inhibitors Latrunculin A or Jasplakinolide (Figs. 6, I - N). From these results, co-treatment with STS and actin polymerization inhibitor was demonstrated to induce elongation of thick and long protrusions.

Co-treatment with STS and CD causes extracellular protrusion of markedly long microtubules

Molecular Pharmacology Fast Forward. Published on February 13, 2015 as DOI: 10.1124/mol.114.096982
This article has not been copyedited and formatted. The final version may differ from this version.

We observed the cell protrusions formed in the presence of both STS and CD using TEM to clarify their constituents. As shown in Fig. 7A, these protrusions formed on HeLa cells were suggested to contain many microtubules that were oriented parallel to the direction of the elongation (left panel, arrowheads). Interestingly, a bulbous expansion, which contains endoplasmic reticulum, ribosomes, and glycogen granules, was observed at the tip of almost all elongated protrusions (middle and right panels). Furthermore, these protrusions were sensitive to the microtubule polymerization inhibitor Nocodazole (Noc) (Fig. 7B). To identify that these protrusions are composed of microtubules, the cells were transfected to express GFP-tubulin and its intracellular localization was observed in living cells with confocal microscopy. Upon co-treatment with STS and CD, GFP-tubulin excessively polymerized to form robust microtubules, and one end of these microtubules protruded outside the cell (Fig. 7C). With stimulation with STS alone, GFP-tubulin polymerized to form microtubules, but these did not protrude outside the cell and did not co-localize with thin actin-based protrusions (Fig. 7D). In steady-state HeLa cells, GFP-tubulin showed a similar localization to endogenous tubulin (Fig. 7E). STS and CD or Noc did not induce appreciable changes in the shape of the nucleus within the observation period. Since the protrusions induced by co-treatment with STS and CD were also susceptible to aldehyde-fixation and alcohol-fixation, as described above (Fig. 3D), we attempted to observe localization of endogenous tubulin using the TCA fixation method. However, anti-tubulin antibodies usable in TCA-fixed cells were not commercially available, and thus we were unable to show localization of endogenous tubulin in these protrusions by immunofluorescent

Molecular Pharmacology Fast Forward. Published on February 13, 2015 as DOI: 10.1124/mol.114.096982
This article has not been copyedited and formatted. The final version may differ from this version.

staining. Next, we investigated the polarity of the extra-long MT-based protrusions. End binding 1 (EB1) is known as a microtubule plus end tracking protein (Mimori-Kiyosue *et al.*, 2000). GFP-tagged EB1 shows an apparent comet moving on microtubules toward their plus end. Thus we observed dynamics of EB1-GFP to investigate the polarity of the growing MT-based protrusions. As shown in Fig. 7F and Movie 4, a large number of comet-like signals were observed in the long elongated protrusions extending from the inside of the cell towards the outside of the cell. As we did not observe EB1-GFP migrating on protrusions towards the inside of the cell, these MT-based protrusions were shown to continuously elongate towards the outside of the cell. In contrast, since the treatment with STS alone did not extend MT-based protrusions towards the outside of the cells, migration of EB1-GFP was limited to the inside of the cell (Fig. 7G). Lastly, we investigated whether there was a correlation between the two types of protrusions elongated in an STS-dependent manner, i.e., the protrusions composed of actin filament and the protrusions composed of microtubule shafts. HeLa cells expressing EB1-GFP were prepared and treated with STS for 60 min, followed by an additional administration of CD. These processes were monitored continuously in living cells. As shown in Fig. 7H, elongation of MT-based protrusions was initiated along with migration of EB1-GFP approximately 3 minutes after addition of CD (arrowheads). These MT-based protrusions elongated independently of the STS-dependent actin-based protrusions (arrows). In addition, CD did not induce contraction of the actin-based protrusions already formed. From these results, the long

Molecular Pharmacology Fast Forward. Published on February 13, 2015 as DOI: 10.1124/mol.114.096982
This article has not been copyedited and formatted. The final version may differ from this version.

MT-based extracellular protrusions were formed by STS treatment under limited G-actin supply condition.

Molecular Pharmacology Fast Forward. Published on February 13, 2015 as DOI: 10.1124/mol.114.096982
This article has not been copyedited and formatted. The final version may differ from this version.

Discussion

Although STS is widely used as an apoptosis inducer, the induction of apoptosis appears to have little association with the formation of protrusions, since induction of the elongation of protrusions required a sufficiently lower concentration of STS than activation of caspase3/7 in the HeLa cells used in this experiment, and the treatment time was also shorter (Fig. 3A). Our result is not contradictory to a number of previous reports in terms of the time course of caspase3/7 activation by STS (Jiang *et al.*, 2013). STS has also been reported to transiently increase of the intracellular ATP level (Zamaraeva *et al.*, 2005), but it was not reproduced in our conditions (Fig. 4F). This may be related to the Warburg effect whereby ATP derived from the glycolytic pathway accounts for around 90% in the cells used in our experiment (Fig. 4A), which is significantly greater than ATP derived from oxidative phosphorylation. STS inhibits the function of proteins dependent on the coenzyme ATP by invading the active center as an ATP mimetic (Duda *et al.*, 2010). In contrast to a report stating that STS facilitates actin polymerization by directly binding to the ATP binding cassette of synapsin I (Defranchi *et al.*, 2010), actin-based protrusions were not extended by STS in the absence of ATP (Fig. 4J). The result suggests that this molecular mechanism involves an ATP-consuming, STS-insensitive factor.

Filopodial protrusions extend against the retrograde actin flow in the steady state (Yamashiro *et al.*, 2014). Many of cellular protrusions involved in cell migration are formed transiently and disappear subsequently. These protrusions rarely exceed 10 μm (Mogilner and Rubinstein, 2005). On the other hand, filopodial protrusions formed

Molecular Pharmacology Fast Forward. Published on February 13, 2015 as DOI: 10.1124/mol.114.096982
This article has not been copyedited and formatted. The final version may differ from this version.

as intercellular communication pathways are known to include long ones (Sanders *et al.*, 2013). Tunneling nanotube (TNT) is a known type of long-chain, actin-based protrusion (Rustom *et al.*, 2004). TNT is a canalicular bridge formed in many cells including neurons and immune cells, and has been reported to be involved in intercellular exchange of organelles and signaling molecules between the bridged cells (Hurtig *et al.*, 2010). Although the mechanism of TNT formation has not been elucidated fully, Cdc42-independent, Myo10- and fascin-dependent, actin-based protrusion has been suggested to be involved therein (Gousset *et al.*, 2013). However, little has been known about the mechanism controlling the length of protrusions (Mogilner and Rubinstein, 2005). While the actin-based protrusions formed upon STS treatment were extremely long, their elongation velocity approximated the velocity of the long protrusions mentioned above (Fig. 1). Moreover, the protrusions found by Sanders *et al*. are susceptible to aldehyde fixation. Because the actin-derived protrusions we obtained are also susceptible to paraformaldehyde fixation, they may have morphological similarities. Only glutaraldehyde (Figs. 3B and 7A) and TCA (Fig. 3D) allowed for fixation of cells while maintaining the protrusion morphologies in this study, but we could hardly conduct any protein localization analysis by immunofluorescence staining, because these fixation methods reduced the antibody recognition ability. Indeed, there was no detectable immunofluorescence staining by using commercially available antibodies against tubulin, fascin, Myo10, myosin II, vimentin, gelsolin, cofilin, and profilin. This may be also a factor preventing analysis of the molecular mechanism.

Many of the signals related to formation of filopodial protrusions are

Molecular Pharmacology Fast Forward. Published on February 13, 2015 as DOI: 10.1124/mol.114.096982
This article has not been copyedited and formatted. The final version may differ from this version.

transmitted through activation of Rho family small GTPases (Mattila and Lappalainen, 2008). In this study, Cdc42-knockdown cells showed no influence on elongation of STS-dependent protrusions (Fig. 5). Thus STS is suggested to target a protein located downstream of Cdc42. N-WASP, an effector of Cdc42, recruits Arp2/3 complex and G-actin through the VCA domain (Miki *et al.*, 1998). The report shows that the expression of VCA domain enhances the formation of actin polymerization nuclei without regulation by Cdc42. In the cells transfected to express the VCA domain, elongation of MT-based protrusions, but of actin-based protrusions, was induced (Fig. S2A). Tubulin stabilization was presumably facilitated by an unknown mechanism, because the VCA domain excluded G-actin required for elongation of actin-based protrusions. This phenomenon was reproduced by using the G-actin-depleting agent LatA or Jsp (Figs. 6, I - N). The presence of an unknown factor recognizing the G-actin level and regulating MT polymerization is predicted, and identification of the factor merits further research.

The signal from small GTPases phosphorylates LIMK through phosphorylation of ROCK and PAK, leading to phosphorylation of cofilin. Dephosphorylated cofilin depolymerizes a part of existing cytoskeleton to secure G-actin, a material for cellular protrusions. Elongation of actin-based protrusions by STS was not suppressed in HeLa cells expressing the S3E mutant of cofilin (Fig. S2B) (Suurna *et al.*, 2006). Because a similar result was obtained in cofilin-knockdown cells (Fig. 5), STS is strongly suggested to induce formation of protrusions in a cofilin-independent manner. Although cellular protrusions can be formed independent

Molecular Pharmacology Fast Forward. Published on February 13, 2015 as DOI: 10.1124/mol.114.096982
This article has not been copyedited and formatted. The final version may differ from this version.

of cofilin *in vitro* (Lee *et al.*, 2010), details of the mechanism underlying cofilin-independent formation of protrusions in live cells have not been elucidated sufficiently.

Ena/VASP is involved in enhancement of actin polymerization and bundling (Bachmann *et al.*, 1999). We prepared two DN mutants of VASP, EVH2- and EVH1-deleted mutants, as well as CA mutant, S157/S239/S278/DDD (Zhuang *et al.*, 2004), and treated the cells expressing each of these mutants with STS. However, no influence on formation of actin-based protrusions was noted (Figs. S2, C - E). Because a similar result was obtained in VASP-knockdown cells (Fig. 5), STS is suggested to act in a VASP-independent manner.

Formin family proteins are involved in enhancement of linearization of AFs through supply of G-actin by profilin (Watanabe *et al.*, 1999). We prepared Y59A, R88L, and H133S mutants of profilin (Wittenmayer *et al.*, 2004), expressed each of them in cells, and stimulated the cells with STS. However, STS induced elongation of actin-based protrusions in all cases (Figs. S2, F - H). Because a similar result was also obtained in profilin-knockdown cells (Fig. 5), STS-induced elongation of actin-based protrusions is suggested to occur independently of the formin-profilin pathway. Formin family proteins have also been reported to contribute to MT stabilization (Chesarone *et al.*, 2010). In this study, MT-based cellular protrusions were not formed even in the presence of CA-DIAPH1 (Fig. S2I) (Palazzo *et al.*, 2001). Further detailed investigation is necessary to determine whether DIAPH1 is involved in elongation of MTs in the extracellular direction.

Molecular Pharmacology Fast Forward. Published on February 13, 2015 as DOI: 10.1124/mol.114.096982
This article has not been copyedited and formatted. The final version may differ from this version.

Bundling of AFs by fascin contributes to formation of stable filopodial protrusions, and the activity is reduced by PKC-catalyzed phosphorylation of the Ser39 residue (Vignjevic *et al.*, 2006). In HeLa cells expressing wild-type fascin, the protrusions extended independently of STS, and fascin was localized in the protrusions (Fig. S2J). In addition, even longer protrusions were formed upon STS stimulation. Even though the S39E mutant does not localize in the protrusions, STS stimulation caused elongation of the protrusions (Fig. S2K). However, because knockdown of endogenous fascin led to suppression of the STS-induced elongation of protrusions (Fig. 5), STS is suggested to be partly involved in the mechanism for the suppressive activity of fascin on the elongation of protrusion in the steady state.

Myo10 is an unconventional motor protein localized in the tips of filopodial protrusions. Although it is considered to be involved in the formation of protrusion, the mechanism is not fully understood (Kerber and Cheney, 2011). Myo10 has also been reported to enhance formation of cellular protrusions when overexpressed (Bohil *et al.*, 2006). The STS-induced elongation of protrusions was partially inhibited by knockdown of endogenous Myo10 (Fig. 5). This suggests that the Myo10 function is also involved in part in the elongation of STS-dependent protrusions. Interestingly, Myo10 has been reported to migrate efficiently on the actin bundle cross-linked by fascin (Nagy *et al.*, 2008). It is suggested that an unknown mechanism is available to suppress excessive elongation of protrusions induced by these proteins and STS acts to deactivate its function. However, identification of the factor requires further investigation.

While STS has been reported to induce formation of branched protrusions in platelets (Nakamura *et al.*, 1995) and cultured neurons (Kitamura *et al.*, 2003), it is unknown whether these protrusions are identical to the linear protrusions observed in the present study. Branched protrusions were not observed in HeLa, COS7, HepG2, or H1299 cells (Figs. 1, G - J). CD-dependent extension of MT-based protrusions in *Drosophila* S2 cells has been reported (Ling *et al.*, 2004), but few findings regarding MTs as cellular protrusions are available. Clostridium difficile toxin (CDT) induces depolymerization of actin through ADP-ribosylation and results in elongation of MT-based protrusions (Schwan *et al.*, 2014). The morphology of protrusions, particularly a globular form at the tip of protrusion, are similar to that observed in the present study (Figs. 6H and 7A). Although the mechanism of MT-based protrusion formation has not been elucidated fully, the interaction between the cortical actin and CLIP170/CLASP2 at the plus end of MT has been suggested to be involved in the elongation of microtubules (Plestant *et al.*, 2014). It remains to be examined further how proteins acting on both actin-based protrusions and MTs (Dent and Gertler, 2003) and MT-associated proteins (MAPs) behave in the presence of STS.

The present work provided us findings suggesting that determination of the length of protrusion is under physiological regulation. Moreover, it is significant to have shown that even MTs are capable of extending as cellular protrusions. The fact that the regulatory factors of these protrusions were modulated by STS-susceptible kinases provides a significant advantage in further elucidation of the mechanism controlling formation and retraction of protrusions.

Molecular Pharmacology Fast Forward. Published on February 13, 2015 as DOI: 10.1124/mol.114.096982
This article has not been copyedited and formatted. The final version may differ from this version.

Acknowledgements

We thank Ryo Miyata, Tsuyoshi Kono, and Takuya Kakuki for helpful discussions and preliminary experiments. We also thank Mikie Kodama from the Kojima laboratory for technical assistance.

Authorship Contributions

Participated in research design and obtained funding: Kohno, Ninomiya, Kojima.

Conducted experiments: Kohno, Ninomiya, Kikuchi, Konno.

Performed data analysis: Kohno Ninomiya, Kikuchi, Konno.

Wrote or contributed to the writing of the manuscript: Kohno, Kojima

Molecular Pharmacology Fast Forward. Published on February 13, 2015 as DOI: 10.1124/mol.114.096982
This article has not been copyedited and formatted. The final version may differ from this version.

References

Bachmann C, Fischer L, Walter U, and Reinhard M (1999) The EVH2 domain of the vasodilator-stimulated phosphoprotein mediates tetramerization, F-actin binding, and actin bundle formation. *J Biol Chem* **274**:23549–23557.

Blanchoin L, Boujemaa-Paterski R, Sykes C, and Plastino J (2014) Actin dynamics, architecture, and mechanics in cell motility. *Physiol Rev* **94**:235–263.

Bohil AB, Robertson BW, and Cheney RE (2006) Myosin-X is a molecular motor that functions in filopodia formation. *Proc Natl Acad Sci U S A* **103**:12411–12416.

Charpentier MS, Whipple R a, Vitolo MI, Boggs AE, Slovic J, Thompson KN, Bhandary L, and Martin SS (2014) Curcumin targets breast cancer stem-like cells with microtentacles that persist in mammospheres and promote reattachment. *Cancer Res* **74**:1250–1260.

Chesarone M a, DuPage AG, and Goode BL (2010) Unleashing formins to remodel the actin and microtubule cytoskeletons. *Nat Rev Mol Cell Biol* **11**:62–74.

Defranchi E, De Franchi E, Schalon C, Messa M, Onofri F, Benfenati F, and Rognan D (2010) Binding of protein kinase inhibitors to synapsin I inferred from pair-wise binding site similarity measurements. *PLoS One* **5**:e12214.

Dent EW, and Gertler FB (2003) Cytoskeletal dynamics and transport in growth cone motility and axon guidance. *Neuron* **40**:209–227.

Dos Remedios CG, Chhabra D, Kekic M, Dedova I V, Tsubakihara M, Berry D a, and Nosworthy NJ (2003) Actin binding proteins: regulation of cytoskeletal microfilaments. *Physiol Rev* **83**:433–473.

Duda T, Yadav P, and Sharma RK (2010) ATP allosteric activation of atrial natriuretic factor receptor guanylate cyclase. *FEBS J* **277**:2550–2553.

Gousset K, Marzo L, Commere P-H, and Zurzolo C (2013) Myo10 is a key regulator of TNT formation in neuronal cells. *J Cell Sci* **126**:4424–4435.

Govek E-E, Newey SE, and Van Aelst L (2005) The role of the Rho GTPases in neuronal development. *Genes Dev* **19**:1–49.

Hayashi K, Yonemura S, Matsui T, Tsukita S, and Tsukita S (1999) Immunofluorescence detection of ezrin / radixin / moesin (ERM) proteins with their carboxyl-terminal threonine phosphorylated in cultured cells and tissues Application of a novel fixation protocol using trichloroacetic acid (TCA) as a fixative. *J Cell Sci* **112**:1149–1158.

Heasman SJ, and Ridley AJ (2008) Mammalian Rho GTPases: new insights into their functions from in vivo studies. *Nat Rev Mol Cell Biol* **9**:690–701.

Hurtig J, Chiu DT, and Onfelt B (2010) Intercellular nanotubes: insights from imaging studies and beyond. *Wiley Interdiscip Rev Nanomed Nanobiotechnol* **2**:260–276.

Jiang P, Wang J, Kang Z, Li D, and Zhang D (2013) Porcine JAB1 significantly enhances apoptosis induced by staurosporine. *Cell Death Dis* **4**:e823.

Karaman MW, Herrgard S, Treiber DK, Gallant P, Atteridge CE, Campbell BT, Chan KW, Ciceri P, Davis MI, Edeen PT, Faraoni R, Floyd M, Hunt JP, Lockhart DJ, Milanov Z V, Morrison MJ, Pallares G, Patel HK, Pritchard S, Wodicka LM, and Zarrinkar PP (2008) A quantitative analysis of kinase inhibitor selectivity. *Nat Biotechnol* **26**:127–132.

Kerber ML, and Cheney RE (2011) Myosin-X: a MyTH-FERM myosin at the tips of filopodia. *J Cell Sci* **124**:3733–3741.

Kitamura Y, Tsuchiya D, Takata K, Shibagaki K, Taniguchi T, Smith M a., Perry G, Miki H, Takenawa T, and Shimohama S (2003) Possible involvement of Wiskott–Aldrich syndrome protein family in aberrant neuronal sprouting in Alzheimer's disease. *Neurosci Lett* **346**:149–152.

Kollman JM, Merdes A, Mourey L, and Agard D a (2011) Microtubule nucleation by γ-tubulin complexes. *Nat Rev Mol Cell Biol* **12**:709–721.

Lee K, Gallop JL, Rambani K, and Kirschner MW (2010) Self-assembly of filopodia-like structures on supported lipid bilayers. *Science* **329**:1341–1345.

Ling S-C, Fahrner PS, Greenough WT, and Gelfand VI (2004) Transport of Drosophila fragile X mental retardation protein-containing ribonucleoprotein granules by kinesin-1 and cytoplasmic dynein. *Proc Natl Acad Sci U S A* **101**:17428–17433.

Mattila PK, and Lappalainen P (2008) Filopodia: molecular architecture and cellular functions. *Nat Rev Mol Cell Biol* **9**:446–454.

Meng W, Mushika Y, Ichii T, and Takeichi M (2008) Anchorage of microtubule minus ends to adherens junctions regulates epithelial cell-cell contacts. *Cell* **135**:948–959.

Miki H, Sasaki T, Takai Y, and Takenawa T (1998) Induction of filopodium formation by a WASP-related actin-depolymerizing protein N-WASP. *Nature* **391**:93–96.

Mimori-Kiyosue Y, Shiina N, and Tsukita S (2000) The dynamic behavior of the APC-binding protein EB1 on the distal ends of microtubules. *Curr Biol* **10**:865–868.

Mogilner a, and Rubinstein B (2005) The physics of filopodial protrusion. *Biophys J* **89**:782–795.

Murphy D a, and Courtneidge S a (2011) The “ins” and “outs” of podosomes and invadopodia: characteristics, formation and function. *Nat Rev Mol Cell Biol* **12**:413–426.

Nagy S, Ricca BL, Norstrom MF, Courson DS, Brawley CM, Smithback P a, and Rock RS (2008) A myosin motor that selects bundled actin for motility. *Proc Natl Acad Sci U S A* **105**:9616–9620.

Nakamura F, Amieva MR, and Furthmayr H (1995) Phosphorylation of threonine 558 in the carboxyl-terminal actin-binding domain of moesin by thrombin activation of human platelets. *J Biol Chem* **270**:31377–31385.

Palazzo a F, Cook T a, Alberts a S, and Gundersen GG (2001) mDia mediates Rho-regulated formation and orientation of stable microtubules. *Nat Cell Biol* **3**:723–729.

Plestant C, Strale P-O, Seddiki R, Nguyen E, Ladoux B, and Mège R-M (2014) Adhesive interactions of N-cadherin limit the recruitment of microtubules to cell-cell contacts through organization of actomyosin. *J Cell Sci* **127**:1660–1671.

Pollard TD (1986) Rate constants for the reactions of ATP- and ADP-actin with the ends of actin filaments. *J Cell Biol* **103**:2747–2754.

Revenu C, Athman R, Robine S, and Louvard D (2004) The co-workers of actin filaments: from cell structures to signals. *Nat Rev Mol Cell Biol* **5**:635–646.

Rotty JD, Wu C, and Bear JE (2013) New insights into the regulation and cellular functions of the ARP2/3 complex. *Nat Rev Mol Cell Biol* **14**:7–12.

Rustom A, Saffrich R, Markovic I, Walther P, and Gerdes H-H (2004) Nanotubular highways for intercellular organelle transport. *Science* **303**:1007–1010.

Sanders T a, Llagostera E, and Barna M (2013) Specialized filopodia direct long-range transport of SHH during vertebrate tissue patterning. *Nature* **497**:628–632.

Schwan C, Kruppke AS, Nölke T, Schumacher L, Koch-Nolte F, Kudryashev M, Stahlberg H, and Aktories K (2014) Clostridium difficile toxin CDT hijacks microtubule organization and reroutes vesicle traffic to increase pathogen adherence. *Proc Natl Acad Sci U S A* **111**:2313–2318.

Someya M, Kojima T, Ogawa M, Ninomiya T, Nomura K, Takasawa A, Murata M, Tanaka S, Saito T, and Sawada N (2013) Regulation of tight junctions by sex

hormones in normal human endometrial epithelial cells and uterus cancer cell line Sawano. *Cell Tissue Res* **354**:481–494.

Suurna M V, Ashworth SL, Hosford M, Sandoval RM, Wean SE, Shah BM, Bamburg JR, Molitoris BA, Maria V, and James R (2006) Cofilin mediates ATP depletion-induced endothelial cell actin alterations. *Am J Physiol Renal Physiol* **290**:F1398–F1407.

Van der Vaart B, Akhmanova A, and Straube A (2009) Regulation of microtubule dynamic instability. *Biochem Soc Trans* **37**:1007–1013.

Vander Heiden MG, Cantley LC, and Thompson CB (2009) Understanding the Warburg effect: the metabolic requirements of cell proliferation. *Science* **324**:1029–1033.

Vasioukhin V, Bauer C, Yin M, and Fuchs E (2000) Directed actin polymerization is the driving force for epithelial cell-cell adhesion. *Cell* **100**:209–219.

Vignjevic D, Kojima S, Aratyn Y, Danciu O, Svitkina T, and Borisy GG (2006) Role of fascin in filopodial protrusion. *J Cell Biol* **174**:863–875.

Watanabe N, Kato T, Fujita a, Ishizaki T, and Narumiya S (1999) Cooperation between mDia1 and ROCK in Rho-induced actin reorganization. *Nat Cell Biol* **1**:136–143.

Wittenmayer N, Jandrig B, Rothkegel M, Arnold W, Haensch W, Scherneck S, Jockusch BM, and Ro R (2004) Tumor Suppressor Activity of Profilin Requires a Functional Actin Binding Site. *Mol Biol Cell* **15**:1600–1608.

Yamashiro S, Mizuno H, Smith MB, Ryan GL, Kiuchi T, Vavylonis D, and Watanabe N (2014) New single-molecule speckle microscopy reveals modification of the retrograde actin flow by focal adhesions at nanometer scales. *Mol Biol Cell* **25**:1010–1024.

Yeung T, Terebiznik M, Yu L, Silvius J, Abidi WM, Philips M, Levine T, Kapus A, and Grinstein S (2006) Receptor activation alters inner surface potential during phagocytosis. *Science* **313**:347–351.

Zamaraeva M V, Sabirov RZ, Maeno E, Ando-Akatsuka Y, Bessonova S V, and Okada Y (2005) Cells die with increased cytosolic ATP during apoptosis: a bioluminescence study with intracellular luciferase. *Cell Death Differ* **12**:1390–1397.

Zhuang S, Nguyen GT, Chen Y, Gudi T, Eigenthaler M, Jarchau T, Walter U, Boss GR, and Pilz RB (2004) Vasodilator-stimulated phosphoprotein activation of serum-response element-dependent transcription occurs downstream of RhoA and is inhibited by cGMP-dependent protein kinase phosphorylation. *J Biol Chem* **279**:10397–10407.

Molecular Pharmacology Fast Forward. Published on February 13, 2015 as DOI: 10.1124/mol.114.096982
This article has not been copyedited and formatted. The final version may differ from this version.

Footnotes

This work was supported in part by grants from the Ministry of Education, Culture, Sports, Science and Technology, Japan. The authors declare no competing financial interests.

Molecular Pharmacology Fast Forward. Published on February 13, 2015 as DOI: 10.1124/mol.114.096982
This article has not been copyedited and formatted. The final version may differ from this version.

Figure Legends

Fig. 1. STS induces elongation of many long cell protrusions.

(A and B) Confocal live cell images of HeLa cells treated with 1 μM STS (A) or DMSO (B) for 30 min, followed by staining with plasma membrane dye FM1-43 (each left panel) or DIC image (each right panel). (C) Time series of DIC images (See Movie 1 and 2). Time, h:mm:ss. (D) Time course of the elongation of protrusions treated with 1 μM STS (closed circles) or DMSO (open circles) on HeLa cells. n = 250 - 300 protrusions, mean ± SD. (E) Dose-dependent increase in length of protrusions with the indicated concentrations of STS treatment for 30 min. n = 200 protrusions, mean ± SD. (F) Confocal live cell images of the basal (left) and intermediate (middle) sections from another portion of the same specimens as in (A). To define the cell edge, left two images were pseudo-colored (basal section is in green, intermediate is in magenta) and merged (right panel). The cell edge is shown in white. (G - J) Confocal live cell images of various cells including 3Y1 (G), COS7 (H), HepG2 (I), and H1299 (J), treated with STS (left panels) or DMSO (right panels) for 60 min, followed by staining with FM1-43. Bars, 20 μm (A - C, and F - J).

Fig. 2. The effect of inhibitors on the formation of the STS-induced protrusions.

Confocal live cell images of HeLa cells treated with the indicated inhibitor for 120 min, followed by an additional administration of STS or DMSO as indicated for 120 min, and subsequently stained with FM1-43. Bars, 20 μm. The graph shows the effect of

Molecular Pharmacology Fast Forward. Published on February 13, 2015 as DOI: 10.1124/mol.114.096982
This article has not been copyedited and formatted. The final version may differ from this version.

different concentrations of inhibitors on the length of STS-induced protrusions. The length was measured from confocal images as above. n = 50 protrusions, mean ± SD. Target site; GSK, SB216763 and LiCL; Myosin II, blebbistatin; Tyr Kinase, genistein; PKC, H-7 and GF109203X; ROCK, Y27632; PLC, U73122; PI3K, wortmannin; ERK1/2, PD98059.

Fig. 3. STS-mediated protrusions are composed of actin filaments.

(A) Caspase activity assay. HeLa cells were treated with the indicated concentrations of STS for 1 h (closed circles), 2 h (open circles), 4 h (closed triangles), or 10 h (open triangles), and analyzed by caspase 3/7-Glo assay. n = 6, mean ± SD. (B) TEM images of cell protrusions in HeLa cells treated with 1 μM STS (left panel, bar; 100 nm) or DMSO (right panel, bar; 10 μm) for 60 min. Arrows, polymerized actin. N, nucleus. (C) Confocal live cell images of HeLa cells expressing GFP-actin (white in left panels and green in right panels) treated with 1 μM STS (upper panels) or DMSO (lower panels) for 60 min, followed by staining with FM4-64. Each right panel is the merged image of GFP-actin (green), FM4-64 (magenta), and H33342 (cyan). Bar, 20 μm. (D) Confocal images of fixed HeLa cells treated with 1 μM STS (left panel) or DMSO (right panel) for 60 min, followed by immunostaining with anti-actin antibody. Bar, 20 μm.

Fig. 4. ATP supply is required for the elongation of STS-dependent cell protrusions.

Molecular Pharmacology Fast Forward. Published on February 13, 2015 as DOI: 10.1124/mol.114.096982
This article has not been copyedited and formatted. The final version may differ from this version.

(A) Quantification of the relative ATP content in HeLa cells treated with or without 2-DG for 120 min. n = 6, mean ± SD. (B - E) Confocal live cell images of HeLa cells treated with (magenta frames) or without (green frames) 2-DG as in (A), followed by an additional administration of STS (B and D) or DMSO (C and E) for 60 min, and subsequently stained with FM1-43 (green) and H33342 (magenta). Bar, 20 μm. (F) Time course of the relative ATP content in HeLa cells cultured in KH buffer for 2 hours (-120 to 0 min), followed by treated with DMSO (open triangles), STS (closed triangles) and DPI in the presence (closed circles) or absence (open circles) of 30 mM glucose (Glc) for the indicated times. n = 6, mean ± SD. (G - I) Confocal live cell images of HeLa cells treated with DPI for 2 hours, followed by an additional administration of DMSO (G), STS (H) or STS + Glc (I) for 60 min, and subsequently stained with FM1-43. Bar, 20 μm. (J) Dot plot of the length of protrusions with mean (bar) under indicated conditions. n > 900 protrusions.

Fig. 5. Myo10 and fascin are involved in the elongation of STS-dependent cell protrusions.

(A) Western blotting of HeLa cells transfected with siRNA as indicated at the bottom of each upper panel. Lane 1, 0 ng; lane 2, 12.5 ng; lane 3, 25 ng; lane 4, 50 ng of siRNA; lane M, protein weight marker. Lower panels, GAPDH as a loading control. A scrambled siRNA was also transfected (right two panels). (B) Dot plot of the length of protrusions with mean (bar) under indicated conditions. RNA interference experiments were carried out in HeLa cells using 12.5 ng of siRNA (singly-transfection) or 25 ng of

Molecular Pharmacology Fast Forward. Published on February 13, 2015 as DOI: 10.1124/mol.114.096982
This article has not been copyedited and formatted. The final version may differ from this version.

siRNAs (co-transfection). n = 600 - 900 protrusions. Student's t-test: *, $p < 0.001$ (n = 30) vs. lane 2; n.s., not significant (n = 30) vs. lane 2.

Fig. 6. An actin polymerization inhibitor induces elongation of thick cell protrusions in the co-presence of STS.

(A and B) Confocal live cell images of HeLa cells treated with 1 μM STS + 1 μM CD (A) or CD alone (B) for 60 min, followed by staining with FM1-43 (green) and H33342 (magenta). The lower panels, corresponding DIC image. (C - E) High-magnification images of cell protrusions in HeLa cells treated with STS + CD (C), STS alone (D), or DMSO (E) for 60 min, followed by staining with FM1-43. (F) Dot plot of the apparent diameter of protrusions with mean (bar) under indicated conditions. n = 165 protrusions; Student's t-test: *, $p < 0.001$ (n = 30). (G) Quantification of the length of protrusions as in (F). n = 64 protrusions, mean ± SD. Student's t-test: *, $p < 0.001$ (n = 30); **, $p < 0.05$ (n = 30). (H) Time series of DIC (lower panels) and confocal (upper panels) images of HeLa cells expressing PH-GFP treated with STS + CD (See Movie 3). Time, h:mm:ss. (I - N) Confocal live cell images of HeLa cells treated with 1 μM STS (I - K) or DMSO (L - N) in the absence (I and L) or presence of latrunculin A (J and M), or jasplakinolide (K and N) for 60 min, followed by staining with FM1-43. Bars, 20 μm (A, B and H - N) and 5 μm (C - E).

Molecular Pharmacology Fast Forward. Published on February 13, 2015 as DOI: 10.1124/mol.114.096982
This article has not been copyedited and formatted. The final version may differ from this version.

Fig. 7. Co-stimulation with STS and CD causes extracellular protrusion of markedly long microtubules.

(A) TEM images of cell protrusions in HeLa cells simultaneous treated with 1 μM STS and 1 μM CD for 60 min. Arrowheads, microtubule. Arrows, ER (yellow); ribosome (green); glycogen granule (magenta). The right panel shows a detail of the tip of microtubule (inset of the middle panel). Bars, 200 nm (left and right); 5 μm (middle). (B) Confocal live cell image of HeLa cells simultaneous treated with STS, CD, and Noc for 60 min, followed by staining with FM1-43 (green) and H33342 (magenta). (C - E) Confocal live cell images of HeLa cells expressing GFP-tubulin (white in left (C and D) or upper (E) panels, green in right (C and D) or lower (E) panels) treated with STS + CD (C), STS alone (D), or DMSO (E) for 60 min, followed by staining with FM4-64 (magenta in right (C and D) or lower (E) panels) and H33342 (cyan, as above). Bar, 20 μm. The lower panels in (C) and (D) are high magnification images of the upper inset. Bar, 5 μm. Note that no MT-based cell protrusion was observed as in (D). (F) Confocal live cell images of HeLa cells expressing EB1-GFP treated with STS + CD for 3.8 hours. Bar, 20 μm. The right panel is a high magnification image of the inset (see Movie 4). Arrowheads, enrichment of the EB1-GFP at microtubule. Bar, 5 μm. (G) Confocal live cell images of HeLa cells expressing EB1-GFP (white in left panel and green in right panel) treated with 1 μM STS for 2 hours, followed by staining with FM4-64 (magenta in right panel). Bar, 5 μm. Note that no MT-based cell protrusion was observed. (H) Time series of confocal images of HeLa cells expressing EB1-GFP

Molecular Pharmacology Fast Forward. Published on February 13, 2015 as DOI: 10.1124/mol.114.096982
This article has not been copyedited and formatted. The final version may differ from this version.

treated with STS for 60 min, followed by an additional administration of CD at the indicated frames. Arrows, actin-based protrusion; arrowheads, MT-based protrusion.

Fig. 1

Molecular Pharmacology Fast Forward. Published on February 13, 2015 as DOI: 10.1124/mol.114.096982
This article has not been copyedited and formatted. The final version may differ from this version.

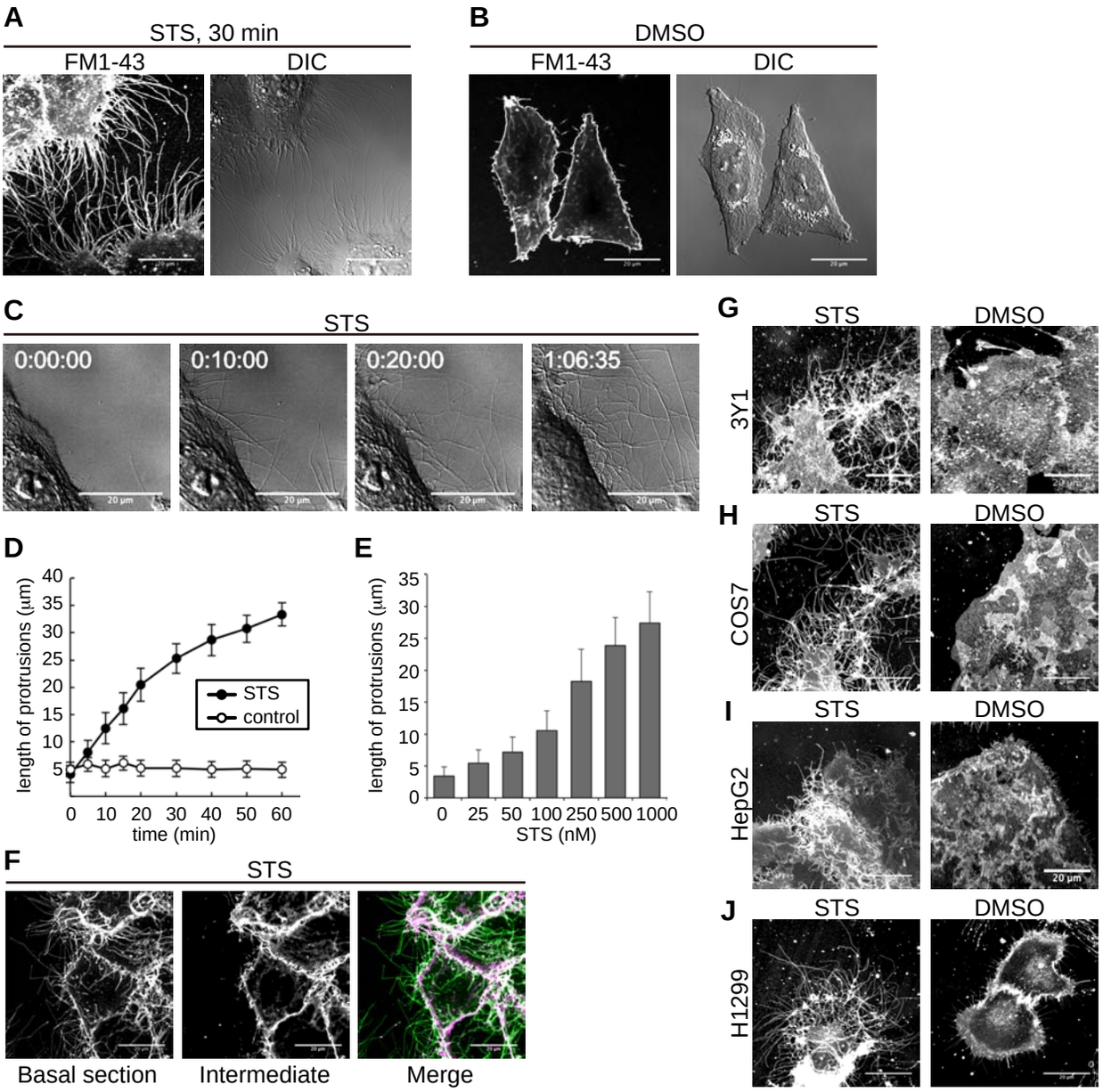

Fig. 2 Molecular Pharmacology Fast Forward. Published on February 13, 2015 as DOI: 10.1124/mol.114.096982
This article has not been copyedited and formatted. The final version may differ from this version.

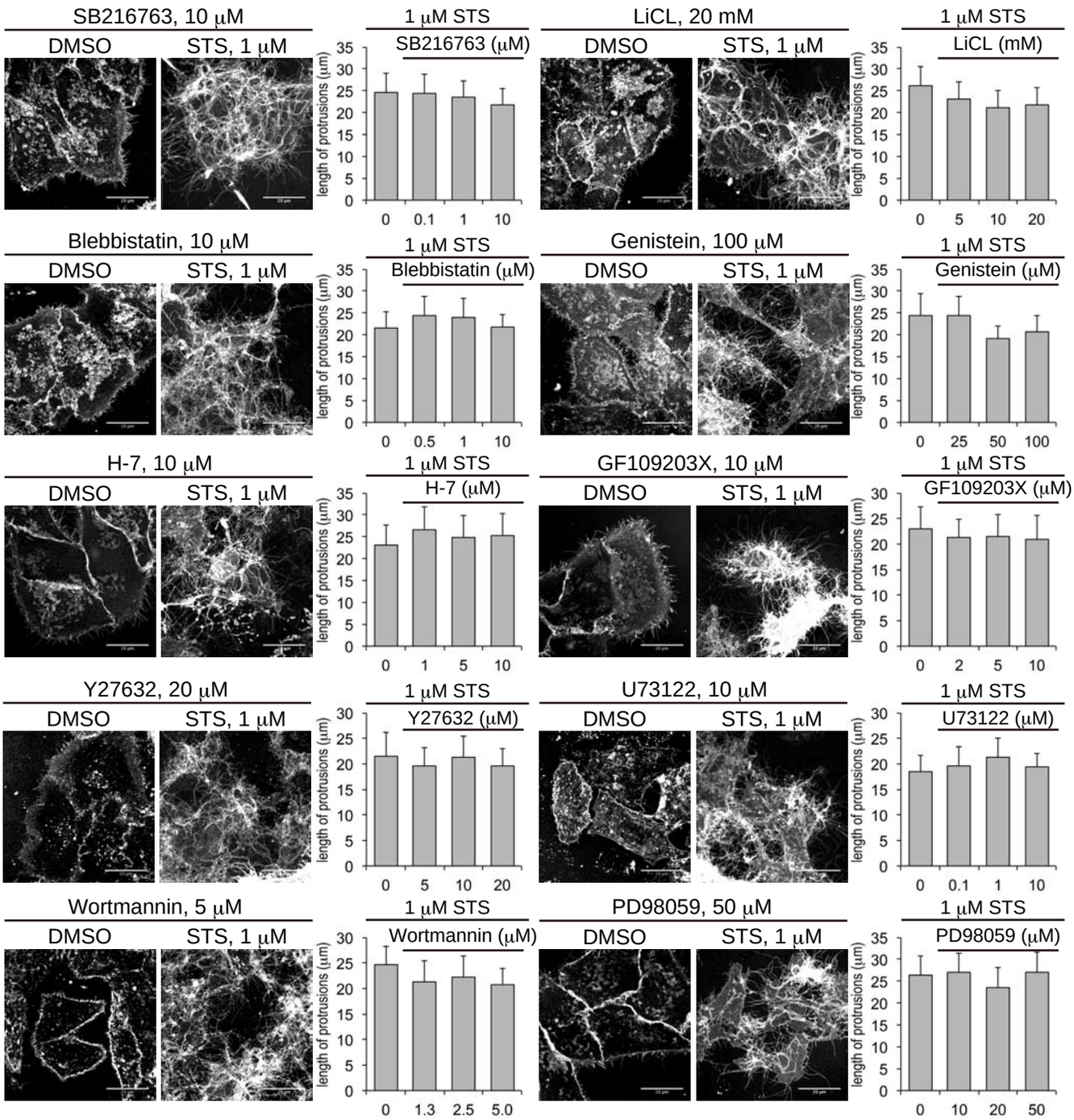

Molecular Pharmacology Fast Forward. Published on February 13, 2015 as DOI: 10.1124/mol.114.096982
This article has not been copyedited and formatted. The final version may differ from this version.

Fig. 3

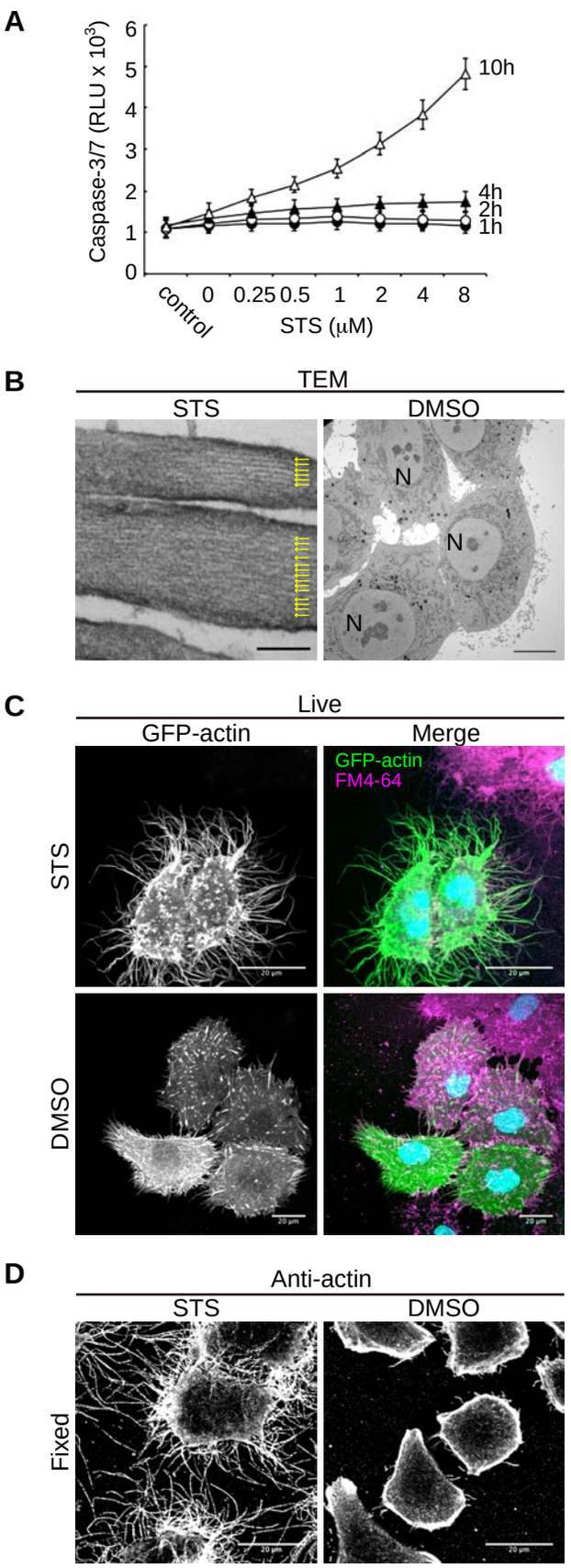

Molecular Pharmacology Fast Forward. Published on February 13, 2015 as DOI: 10.1124/mol.114.096982
This article has not been copyedited and formatted. The final version may differ from this version.

Fig. 4

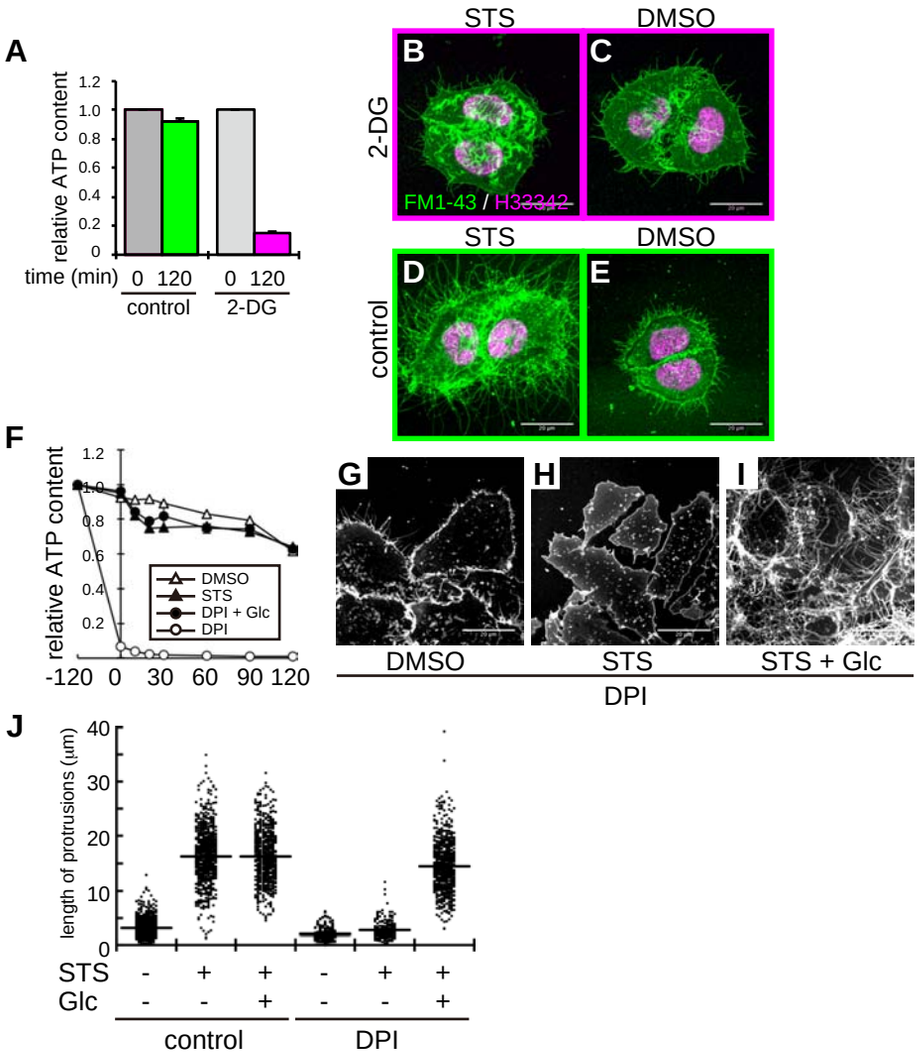

Fig. 5

Molecular Pharmacology Fast Forward. Published on February 13, 2015 as DOI: 10.1124/mol.114.096982
This article has not been copyedited and formatted. The final version may differ from this version.

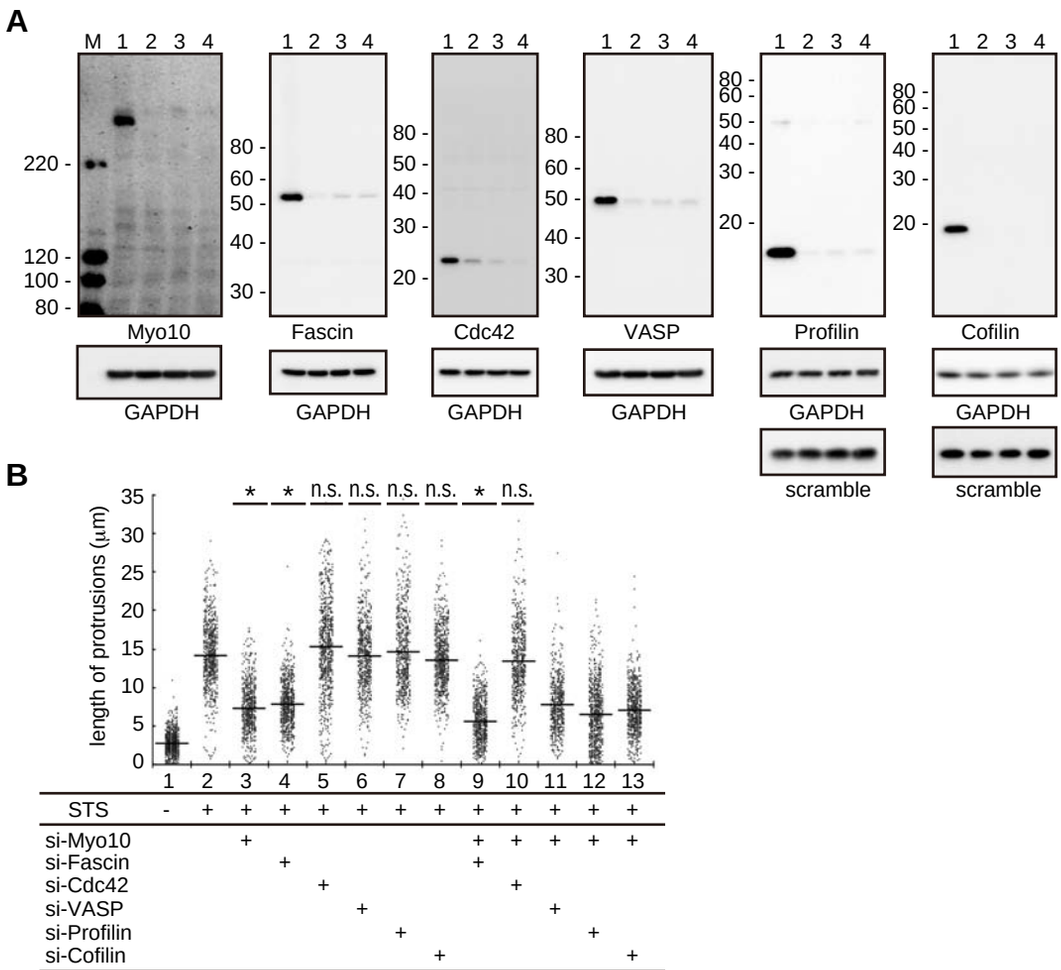

Fig. 6

Molecular Pharmacology Fast Forward. Published on February 13, 2015 as DOI: 10.1124/mol.114.096982
This article has not been copyedited and formatted. The final version may differ from this version.

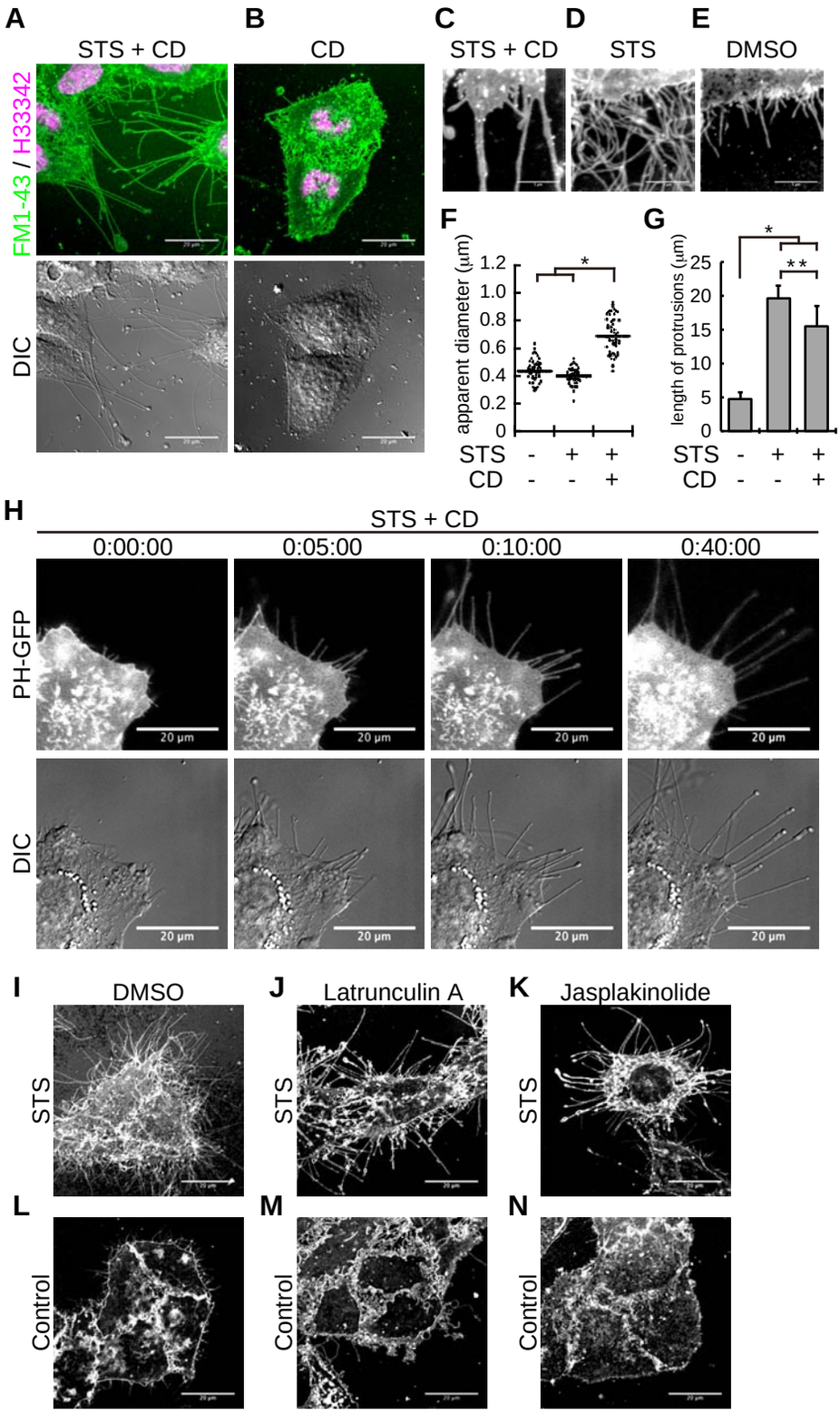

Fig. 7

Molecular Pharmacology Fast Forward. Published on February 13, 2015 as DOI: 10.1124/mol.114.096982
This article has not been copyedited and formatted. The final version may differ from this version.